AD-A132 103 ASYMPTOTIC HIGH FREQUENCY TECHNIQUES FOR UHF AND ABOVE ANTENNAS(U) OHIO STATE UNIV COLUMBUS ELECTROSCIENCE LAB W D BURNSIDE ET AL. MAY 77 ESL-4508-5 N00123-76-C-1371 1/1

UNCLASSIFIED F/G 9/5 NL

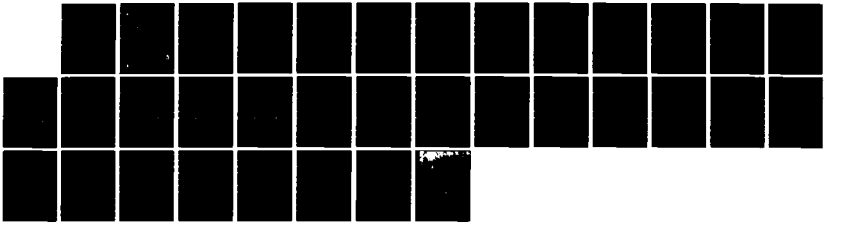

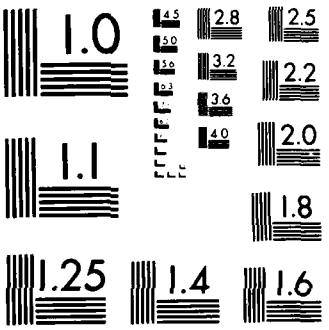

ASYMPTOTIC HIGH FREQUENCY TECHNIQUES FOR UHF AND ABOVE ANTENNAS

Third Quarterly Report - 1 February to 30 April 1977

W.D. Burnside
R.G. Kouyoumjian
R.J. Marhefka
R.C. Rudduck
C.H. Walter

The Ohio State University

ElectroScience Laboratory

Department of Electrical Engineering
Columbus, Ohio 43212

Report 4508-5

Contract N00123-76-C-1371

May 1977

Approved for public release;
distribution unlimited.

Naval Regional Procurement Office
Long Beach, California 90822

NOTICES

When Government drawings, specifications, or other data are used for any purpose other than in connection with a definitely related Government procurement operation, the United States Government thereby incurs no responsibility nor any obligation whatsoever, and the fact that the Government may have formulated, furnished, or in any way supplied the said drawings, specifications, or other data, is not to be regarded by implication or otherwise as in any manner licensing the holder or any other person or corporation, or conveying any rights or permission to manufacture, use, or sell any patented invention that may in any way be related thereto.

UNCLASSIFIED

SECURITY CLASSIFICATION OF THIS PAGE (When Data Entered)

REPORT DOCUMENTATION PAGE

READ INSTRUCTIONS BEFORE COMPLETING FORM

1 REPORT NUMBER	2 GOVT ACCESSION NO. AD-A132 103
	3 RECIPIENT'S CATALOG NUMBER
4 TITLE (and Subtitle) ASYMPTOTIC HIGH FREQUENCY TECHNIQUES FOR UHF AND ABOVE ANTENNAS	5 TYPE OF REPORT & PERIOD COVERED Third Quarterly Report 2/1/77 - 4/30/77
	6 PERFORMING ORG REPORT NUMBER ESL 4508-5
7 AUTHOR(s) W.D. Burnside, R.C. Rudduck, R.G. Kouyoumjian, C.H. Walter, R.J. Marhefka	8 CONTRACT OR GRANT NUMBER(s) Contract N00123-76-C-1371
9 PERFORMING ORGANIZATION NAME AND ADDRESS The Ohio State University ElectroScience Laboratory, Department of Electrical Engineering Columbus, Ohio 43212	10 PROGRAM ELEMENT, PROJECT, TASK AREA & WORK UNIT NUMBERS
11 CONTROLLING OFFICE NAME AND ADDRESS Naval Regional Procurement Office Long Beach, California 90822	12 REPORT DATE May 1977
	13 NUMBER OF PAGES 29
14 MONITORING AGENCY NAME & ADDRESS(if different from Controlling Office)	15 SECURITY CLASS. (of this report) Unclassified
	15a DECLASSIFICATION/DOWNGRADING SCHEDULE

16 DISTRIBUTION STATEMENT (of this Report)

Approved for public release;
distribution unlimited.

17 DISTRIBUTION STATEMENT (of the abstract entered in Block 20, if different from Report)

18 SUPPLEMENTARY NOTES

19 KEY WORDS (Continue on reverse side if necessary and identify by block number)

Computer code
Algorithm
Geometrical Theory of Diffraction
Far Field Pattern
Reflector Antenna
Aperture integration
Cylinders

20 ABSTRACT (Continue on reverse side if necessary and identify by block number)

The overall scope of the program on Contract No. N00123-76-C-1371 between The Ohio State University ElectroScience Laboratory and the Naval Electronics Laboratory Center is to develop the necessary theory, algorithms and computer codes for simulating antennas at UHF and above in a complex ship environment. The work consists of a) basic scattering code development, b) reflector antenna code development and c) basic studies to support items a) and b). This report describes the progress in each of these three areas for the period 1 February 1977 to 30 April 1977.

DD FORM 1 JAN 73 1473 EDITION OF 1 NOV 65 IS OBSOLETE

UNCLASSIFIED

SECURITY CLASSIFICATION OF THIS PAGE (When Data Entered)

TABLE OF CONTENTS

		Page
I	INTRODUCTION	1
II	PROGRAM SCOPE	1
III	BASIC SCATTERING CODE DEVELOPMENT	5
IV	REFLECTOR ANTENNA CODE DEVELOPMENT	15
	A. Rectangular Subaperture Method	15
	B. Program Performance Specification (PPS) for Reflector Antenna Code/Far Field w/o Blockage	21
V	THEORETICAL STUDIES	28
REFERENCE		29

I. INTRODUCTION

This report describes the work done on Contract No. N00123-76-C-1371 for the period 1 February 1977 to 30 April 1977.

The overall program is divided into three areas. These are 1) basic scattering code development, 2) reflector antenna code development and 3) basic theoretical studies to support the first two areas. The following sections describe the progress made during the second quarter in each of the three areas mentioned above.

II. PROGRAM SCOPE

The scope of the work under Contract No. N00123-76-C-1371 is to develop the necessary theory, algorithms and computer codes for simulating antennas at UHF and above in a complex ship environment. A milestone chart for the total program, which extends over a three year period, is shown in Table I. A more detailed breakdown of the effort planned for the first year is shown in Table II. The following sections describe the progress made during the third quarter of the program in Table II.

TABLE I

MILESTONE CHART FOR TOTAL PROGRAM

Task	Time: 1st year	2nd year	3rd year
1. BASIC SCATTERING CODE DEVELOPMENT			
a. Flat plate, box and cylinder independently analyzed for far field effects	---------		
	————————		
b. Coupled solution for flat plate, box and cylinder - far field		---------	
		————	
c. Near field analysis of coupled structures including coupled antennas.		----------	
			————
2. REFLECTOR ANTENNA CODE DEVELOPMENT			
a. General reflector, no blockage, far field	----------		
	————————		
b. General reflector, no blockage, near field		---------	
		————	
c. General reflector with scattering from feed, supports, subreflectors and ship structure		----------	
			————

--------- Theoretical development

———— Formulate algorithms and write and implement computer codes

TABLE II

ASYMPTOTIC HIGH FREQUENCY TECHNIQUES
FOR UHF AND ABOVE ANTENNAS

FIRST YEAR WORK PLAN

	1st Quarter	2nd Quarter
Topic	Task	Task
1. Basic Scattering Code Development		
	FF Flat Plate (T,A)	FF Box (T,A)
	FF CYLINDER (T,A)	FF Cylinder (T,A)
2. Reflector Antenna Code Development		
	General reflector	General reflector
	FF w/o blockage (T)	FF w/o blockage (T)
3. Theoretical Studies		
	Slope Diffraction (T)	Vertex Diffraction (T)

T - Theory

A - Algorithm

U - Code with User's Manual

TABLE II (Contd.)

ASYMPTOTIC HIGH FREQUENCY TECHNIQUES
FOR UHF AND ABOVE ANTENNAS

FIRST YEAR WORK PLAN

Topic	3rd Quarter Task		4th Quarter Task	
1. Basic Scattering Code Development				
	FF Fox	(A,U)	FF Box	(U)
	FF Cylinder	(A,U)	FF Cylinder	(U)
Plate, Box, Cylinder	Coupled FF	(T,A)	Coupled FF	(T,A)
2. Reflector Antenna Code Development				
	General Reflector		General Reflector	
	FF w/o blockage	(T,A)	FF w/o blockage	(A,U)
	General Reflector		General Reflector	
	NF w/o blockage	(T)	NF w/o blocakge	(T)
3. Theoretical Studies				
	Vertex Diffraction	(T)	Vertex Diffraction	(T)

III. BASIC SCATTERING CODE DEVELOPMENT

The purpose of this section is to describe the present status of the basic scattering code development for the analysis of antennas in a complex shipboard environment. The Geometrical Theory of Diffraction (GTD) is being used to develop algorithms to solve for the scattering from basic plate and cylinder structures. These simple components can then be combined to form box-like structures with nearby finite elliptic cylinders that can represent the various component structures of a ship. The algorithms are being implemented into a user-oriented computer code.

In this period the scattering code for the flat plate simulation of convex structures has been completed and delivered to NOSC. A draft copy of a user's manual also was delivered and the scattering code has been succesfully implemented on the NOSC computer system.

The early delivery of the computer code has allowed discussions to take place that will aid in the development of future codes to better satisfy the specific needs of NOSC and other users. For example, an infinite ground plane option has been added to the code now under development based on the needs of NOSC.

The methodology used to input the data into the scattering code also is under revision at present. Default input data are being placed into the program for specific geometries. Commands are being supplied so that only select pieces of data need to be changed for any particular computer run.

The scattering code presently under development will incorporate all of the above improvements. Also, the scope and generality of the problems that can be solved will be increased. The code will allow flat plate simulation of convex and concave structures, finite elliptic cylinder structures, and a psuedo combination of plates and a cylinder structure. However, the coupling between the plate structures and cylinder is not included at this time.

The scattering code for the flat plate simulation of concave structures is being developed to allow as much generality as possible in defining scattering structures by flat plates. This generality also leads to more complexity in the number of coupling terms between the plates. The dominent scattered field components up to the second order of interactions have been added. This would include, for example, double reflected fields between the plates, etc. If a particular geometry of plates is desired that requires higher order scattering terms to obtain a solution useful for engineering purposes, the necessary terms can be easily added after they have been put into the GTD format.

One such term that is not included at present, but has been found to be important, is doubly-diffracted fields. A theoretical study has been under way to show the validity of the GTD in handling double-diffraction. However, if the doubly-diffracted fields are included in all desired regions of space, the algorithm would be very time consuming and hence costly to run. This can be overcome by writing the algorithm in such a way that the doubly-diffracted fields are included only when their effects are significant in the antenna pattern. Techniques to accomplish this have already been initiated, but to fully complete and test them will require additional time and effort.

The scattering code for the finite elliptic cylinder has been assembled and is presently being tested. Improvements were made in the algorithms this past period to improve the efficiency and extend the range of applicability of the code. To illustrate the wide range of cylinder sizes and source distances that can be calculated with this scattering code, a series of radiation patterns for the geometry shown in Figure 1 is presented.

The first set of patterns is for a $\lambda/2$ dipole antenna, mounted parallel to the y-axis at a fixed distance one wavelength from the surface of a perfectly conducting circular cylinder. The antenna pattern for this geometry without a cylinder present is shown in Figure 2. With the dipole oriented parallel to the y-axis the energy propagates around the cylinder following the acoustically hard boundary condition where the electric field is perpendicular to the cylinder surface. The cylinder radius is increased geometrically by a factor of two from a = $1/2\lambda$ to 64λ and the results are shown in Figure 3. All the results are shown in terms of dB plots normalized to 0 dB with 10 dB per division.

Note that there is a slope discontinuity in Figures 3f-h at approximately the $\phi = 90° - 120°$ and $\phi = 240° - 270°$ regions. This is due to the fact that the dipole field can produce a slope field associated with the transition field of the cylinder. This slope transition field has not been added at this time. It is presently under development for another contract and can be added when completed if it appears necessary to give good engineering results.

In Figure 4 the cylinder has a fixed radius of 2λ and the source position is varied $1/2\lambda$, 2λ, 4λ, 8λ off the cylinder surface, respectively.

The results in Figures 5 and 6 are the same as in the above figures except that the dipole is now oriented parallel to the cylinder axis. This represents the acoustically soft boundary condition where the electric field is parallel to the surface of the cylinder. Note that the slope-transition field is not needed in this case because the source field, which is isotropic in the x-y plane for this case, does not have a slope associated with it. Further tests are being made on the scattering code and they will be presented in later reports.

The psuedo combination of plate structures and a finite elliptic cylinder is also being tested at the present time. This part of the scattering code does not contain the interactions between the plates and cylinder; however, the scattered fields from the plates are shadowed by the cylinder and vice versa. This causes discontinuities in the calculated pattern, but this can be very informative. The magnitude of the discontinuity gives a gauge on how important the different coupling fields will be to the final pattern. A start has been made on studying some of these coupling terms but due to the generality the geometries desired and the complexity of finding many of these terms great care will have to be taken in using only those terms necessary for a good engineering result for practical structures. Which terms to use will become clearer as the study progresses during the next contract year.

A user's manual will be completed in the next period for the plates and cylinder scattering code, and the scattering code will be tested and prepared for delivery to NOSC by the end of this contract year.

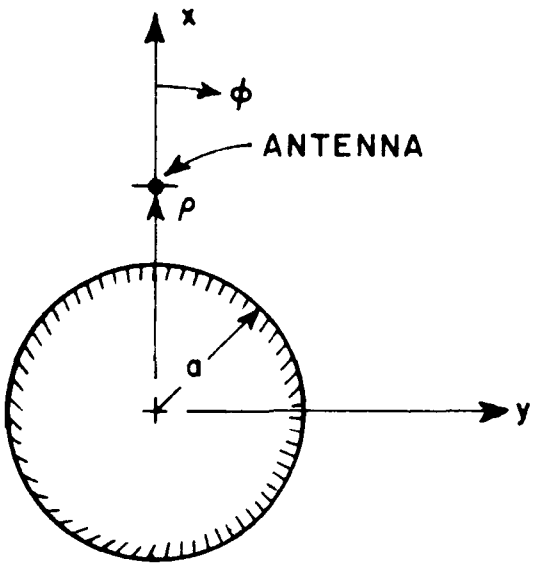

Figure 1. Geometry for antenna mounted near a circular cylinder.

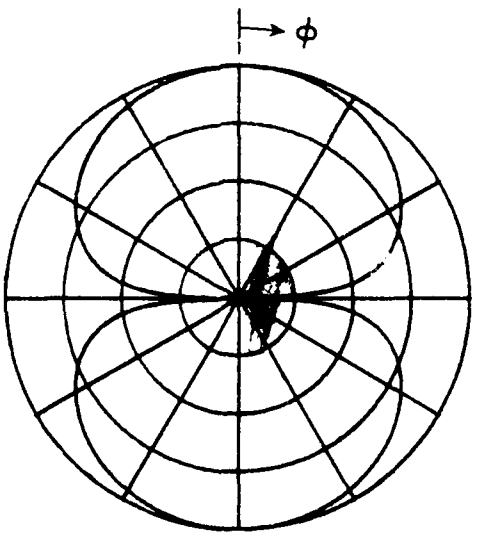

Figure 2. Source radiation pattern in dB for a $\lambda/2$ dipole mounted parallel to the y-axis as shown in Figure 1.

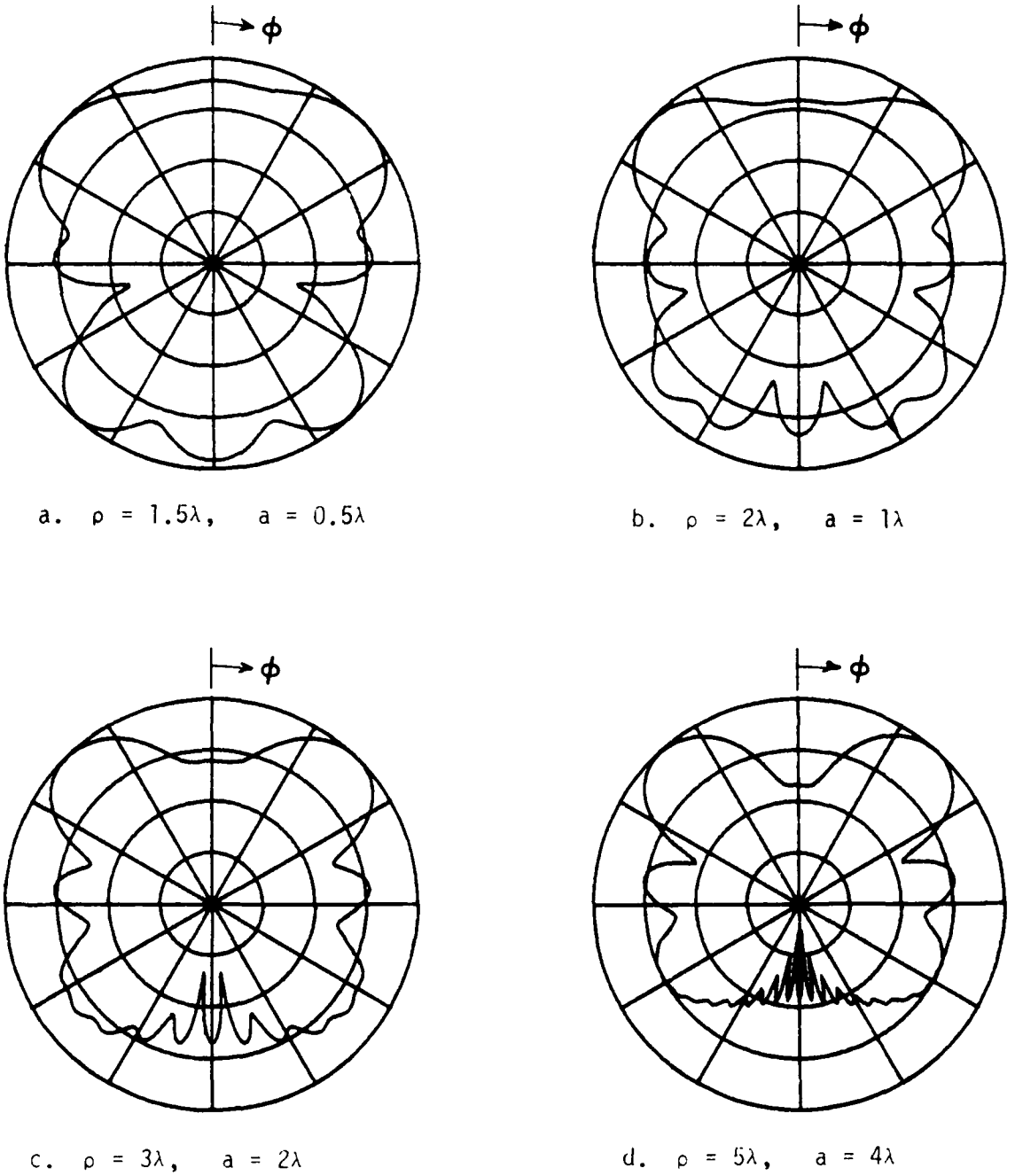

a. $\rho = 1.5\lambda$, $a = 0.5\lambda$

b. $\rho = 2\lambda$, $a = 1\lambda$

c. $\rho = 3\lambda$, $a = 2\lambda$

d. $\rho = 5\lambda$, $a = 4\lambda$

Figure 3. Radiated field of a $\lambda/2$ dipole mounted parallel to the y-axis one wavelength from the surface of a circular cylinder of radius a plotted in dB.

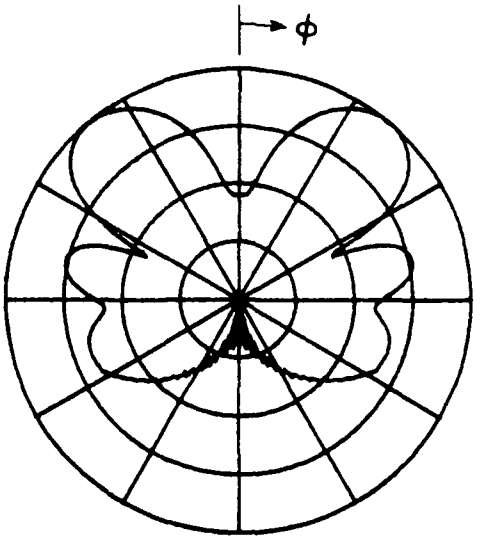

e. $\rho = 9\lambda$, $a = 8\lambda$

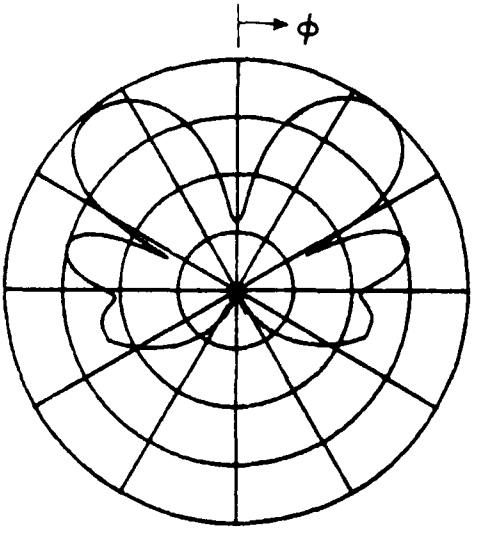

f. $\rho = 17\lambda$, $a = 16\lambda$

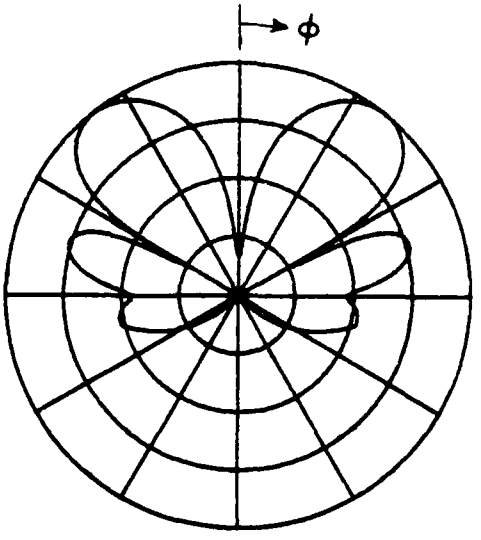

g. $\rho = 33\lambda$, $a = 32\lambda$

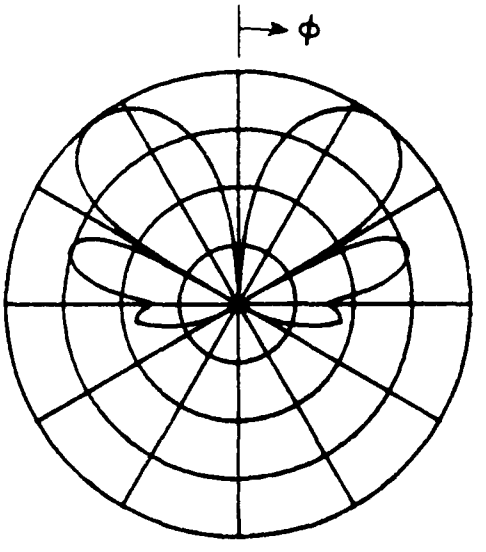

h. $\rho = 65\lambda$, $a = 64\lambda$

Figure 3. (Continued)

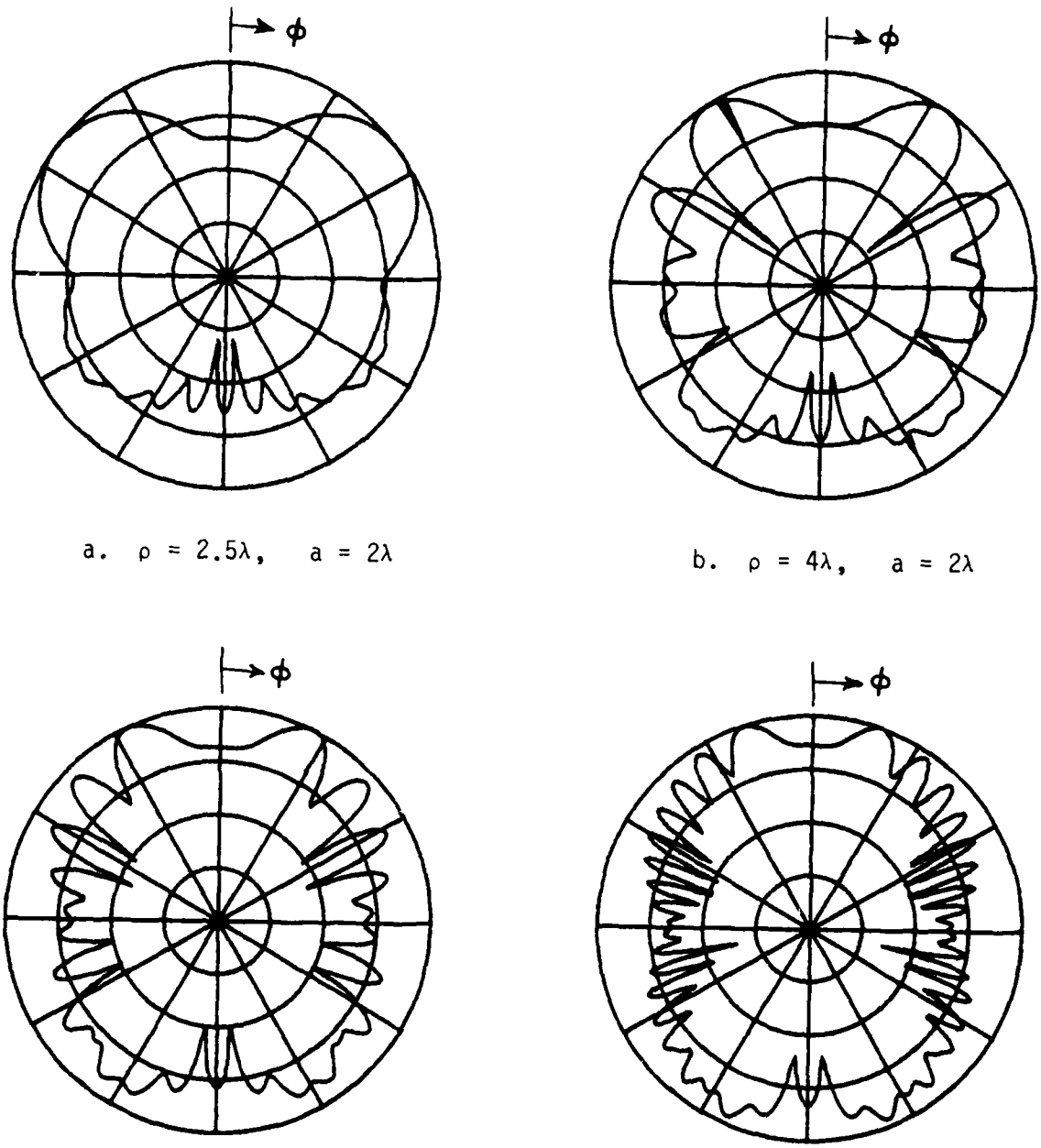

a. $\rho = 2.5\lambda$, $a = 2\lambda$

b. $\rho = 4\lambda$, $a = 2\lambda$

c. $\rho = 6\lambda$, $a = 2\lambda$

d. $\rho = 10\lambda$, $a = 2\lambda$

Figure 4. Radiated field of a $\lambda/2$ dipole mounted parallel to the y-axis a distance ρ from the center of a circular cylinder of two wavelength radius plotted in dB.

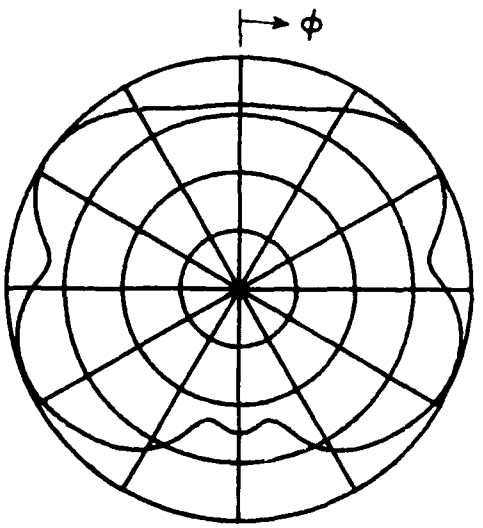

a. $\rho = 1.5\lambda$, $a = 0.5\lambda$

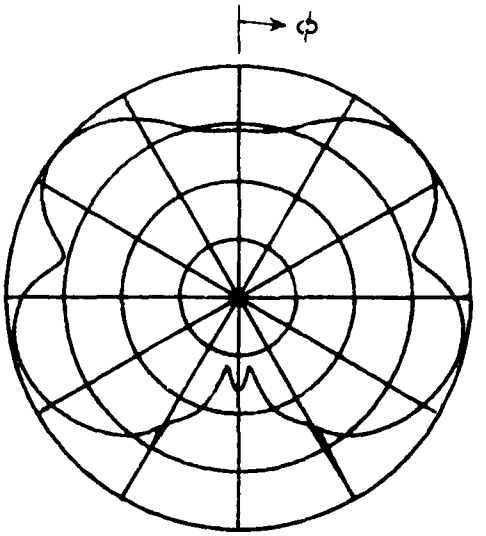

b. $\rho = 2\lambda$, $a = 1\lambda$

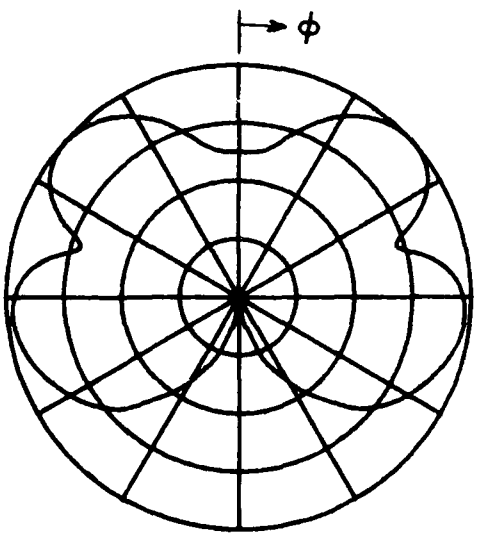

c. $\rho = 3\lambda$, $a = 2\lambda$

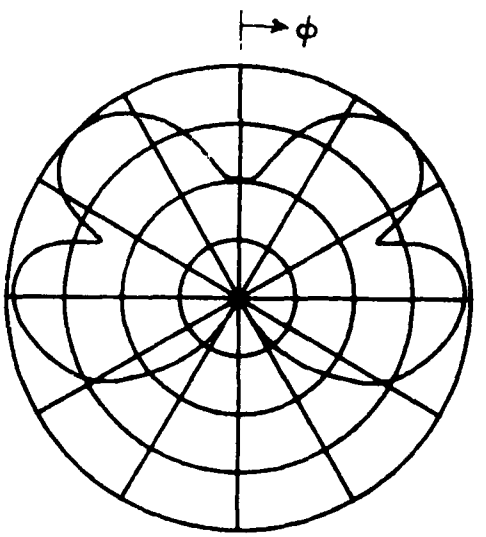

d. $\rho = 5\lambda$, $a = 4\lambda$

Figure 5. Radiated field of a $\lambda/2$ dipole mounted parallel to the cylinder axis one wavelength from the surface of a circular cylinder of radius a plotted in dB.

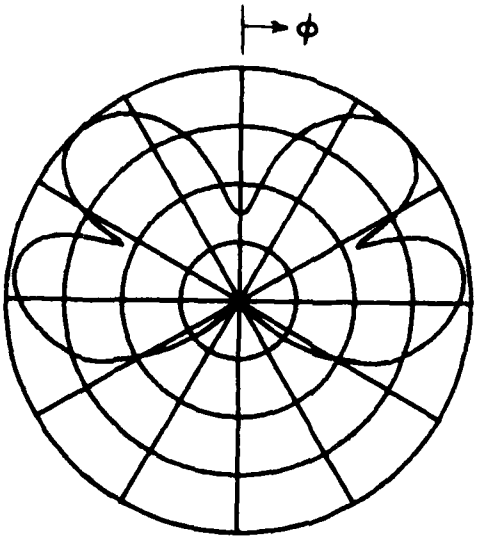

e. $\rho = 9\lambda$, $a = 8\lambda$

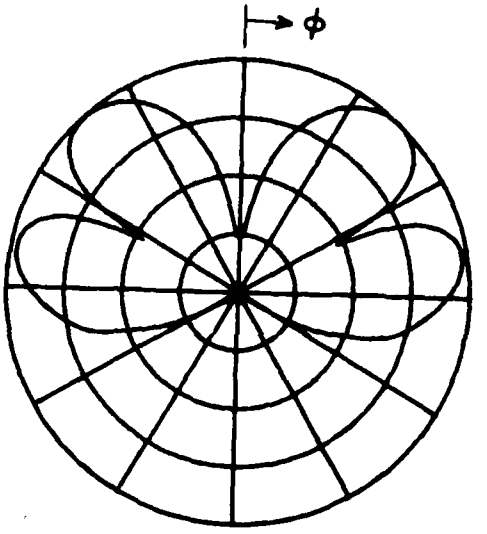

f. $\rho = 17\lambda$, $a = 16\lambda$

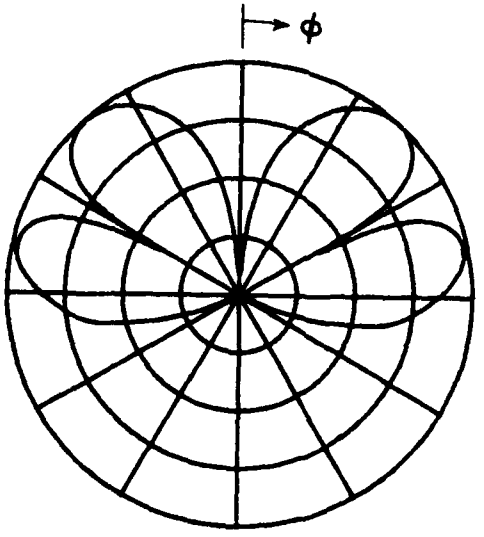

g. $\rho = 33\lambda$, $a = 32\lambda$

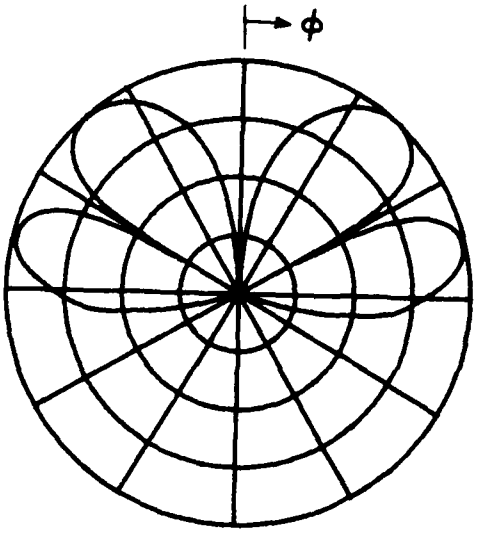

h. $\rho = 65\lambda$, $a = 64\lambda$

Figure 5. (Continued)

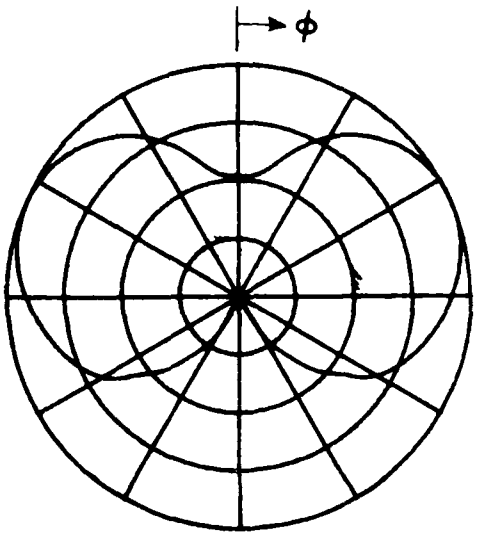

a. $\rho = 2.5\lambda$, $a = 2\lambda$

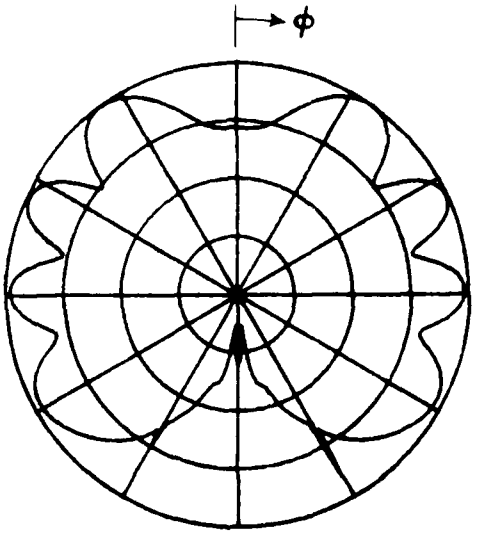

b. $\rho = 4\lambda$, $a = 2\lambda$

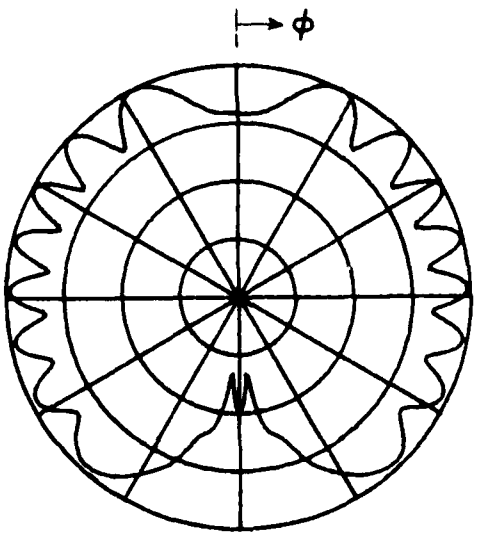

c. $\rho = 6\lambda$, $a = 2\lambda$

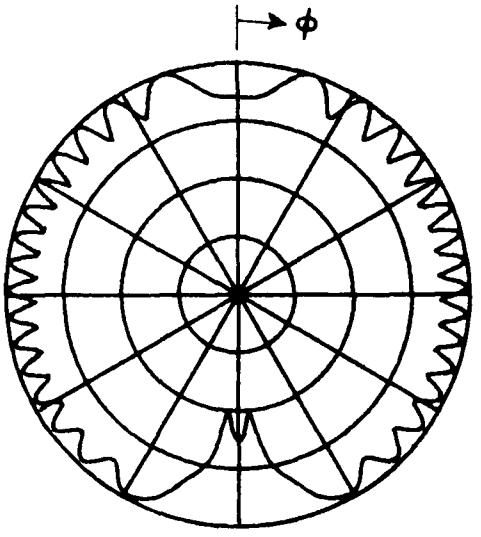

d. $\rho = 10\lambda$, $a = 2\lambda$

Figure 6. Radiated field of a $\lambda/2$ dipole mounted parallel to the y-axis a distance ρ from the center of a circular cylinder of two wavelength radius plotted in dB.

IV. REFLECTOR ANTENNA CODE DEVELOPMENT

The purpose of the present effort is to develop a user-oriented computer program package by which the far field pattern of a typical Navy reflector antenna can be calculated. Feed blockage and scattering effects are not included in this phase. These will be included later (see Table III).

Development of the applied theory to be used in the computer program package for the general reflector antenna has continued. As reported in the Second Quarterly Report (1 November to 31 January 1977), the use of overlapping subapertures with triangular distribution provides an accurate method for calculating the far field pattern while minimizing the number of aperture field computations.

The computer algorithms for the aperture integration (AI) part of the reflector antenna computer code for the far field pattern are being programmed on the OSU Datacraft computer. Programming of several portions of the computer code has been completed. One portion involves inputting a general reflector rim shape and then subdividing the aperture into rectangular subapertures. Another portion performs the 2-D numerical integration required to calculate the far field pattern.

The theory of the rectangular subaperture method is given below. Following that, the program performance specification (PPS) for the reflector antenna computer code (FF w/o blockage) is given.

A. Rectangular Subaperture Method

The theoretical approach for computing the far field pattern of the general reflector is based on a combination of the Geometrical Theory of Diffraction (GTD) and Aperture Integration (AI) techniques. AI is used to compute the main beam and near sidelobes; GTD is used to compute the wide-angle sidelobes and the backlobes. The geometry of the reflector rim is treated as piece-wise linear; that is, a series of linear segments is used to approximate a smoothly curved rim such as a circular aperture.

Although GTD is used to calculate most of the far field pattern, the main beam and near sidelobes of the reflector antenna are calculated by the aperture integration approach. Since the required integration is usually very cumbersome for electrically large antennas, an approach based on using overlapping rectangular subapertures is used. Each subaperture can be electrically large, i.e., several wavelengths in size. This minimizes the number of subapertures required. The theory of the rectangular subaperture method for aperture integration will now be given.

The reflector rim geometry is specified by the x- and y-coordinates of each junction point L_k and U_n on the lower and upper portions of the rim, respectively. Thus the projection of the reflector rim onto the aperture plane is specified as piece-wise linear. A typical reflector rim shape is

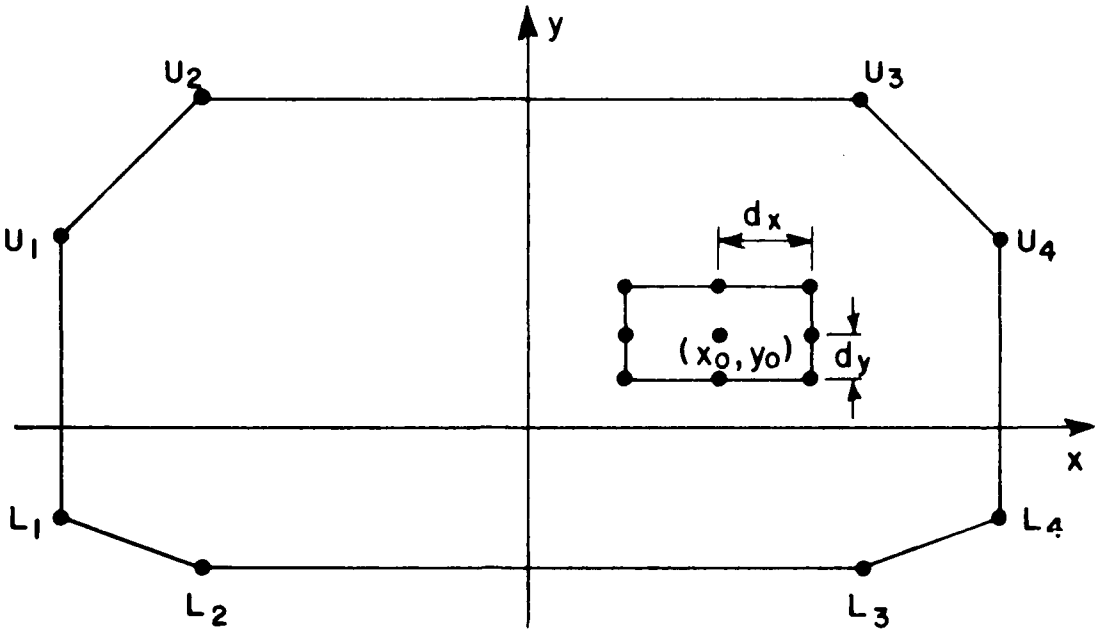

(a)

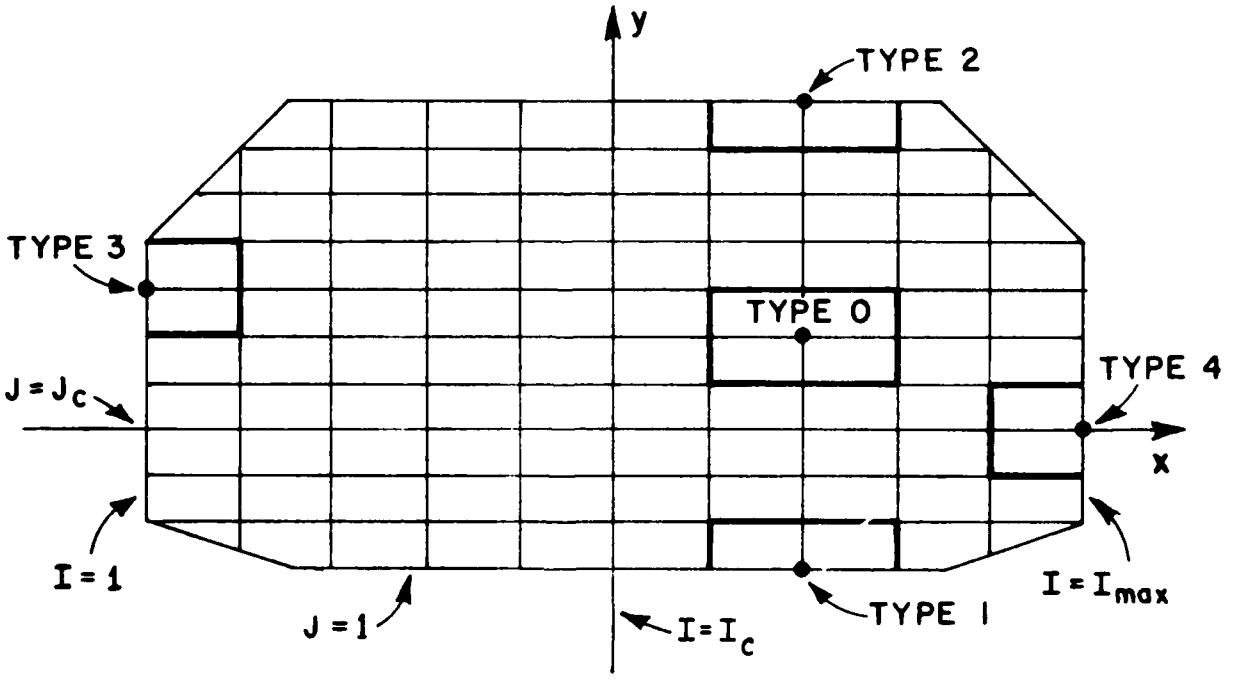

(b)

Figure 7. Reflector rim geometry and rectangular subapertures.

shown in Figure 7a, with four points on each of its lower and upper portions. A rectangular grid size (dx and dy) is then chosen so that the aperture can be divided into rectangular subapertures. A typical subaperture is shown in Figure 7a where the aperture field distribution is specified by its value at the center of the subaperture and by its values at the 8 points on the edge of subaperture (centers for the overlapping subapertures) as shown in Figure 7a. Thus the distribution over the entire aperture plane is specified by its values on the rectangular grid as shown in Figure 7b. The vertical grid lines are numbered by integer values of I = 1 to I_{max} corresponding to the x-coordinate as shown in Figure 7b. The horizontal grid lines corresponding to the y-coordinate are numbered by the integer J, starting with J = 1 for the lowest point on the rim. The center of the aperture plane, which is on the z axis of the reflector, is designated by $I = I_C$ and $J = J_C$ as shown. The minimum and maximum values of J on each vertical grid line (I) are determined by the rim geometry.

The y-coordinates of the intersection of the lower rim and the vertical grid line (I) is designated by Y_L as shown in Figure 8. The horizontal grid line closest to this intersection is designated by $J = J_{LR}(I)$. Similarly, the horizontal grid closest to the intersection (at Y_U) of the same vertical grid line with the upper rim is designated by $J = J_{UR}(I)$. In the computer code the array variables $J_{LR}(I)$ and $J_{UR}(I)$ serve as the lower and upper limits of the y-integration for each vertical grid line (I).

The aperture distribution for the basic subaperture (Type 0) is a triangular one as given by

$$f_{so}(x,y) = \left(1 - \frac{|x-x_o|}{d_x}\right)\left(1 - \frac{|y-y_o|}{d_y}\right) \qquad (1)$$

for $|x-x_o| < d_x$ and $|y-y_o| < d_y$; and f_{so} is zero otherwise. The resulting far field pattern for the basic subaperture, i.e., the element pattern, is given by

$$F_{so}(0,\phi) = dx\ dy \left[\frac{\sin(\frac{\phi x}{2})}{(\frac{\phi x}{2})}\right]^2 \left[\frac{\sin(\frac{\phi y}{2})}{(\frac{\phi y}{2})^2}\right]^2 \qquad (2)$$

where

$$\phi x = k\ d_x\ \sin\theta\ \cos\phi$$

and

$$\phi y = k\ d_y\ \sin\theta\ \sin\phi\ .$$

The phase reference for Equation (2) is taken at the center of the sub-aperture (x_o, y_o); the phase is referred to the origin of the aperture plane during the integration process.

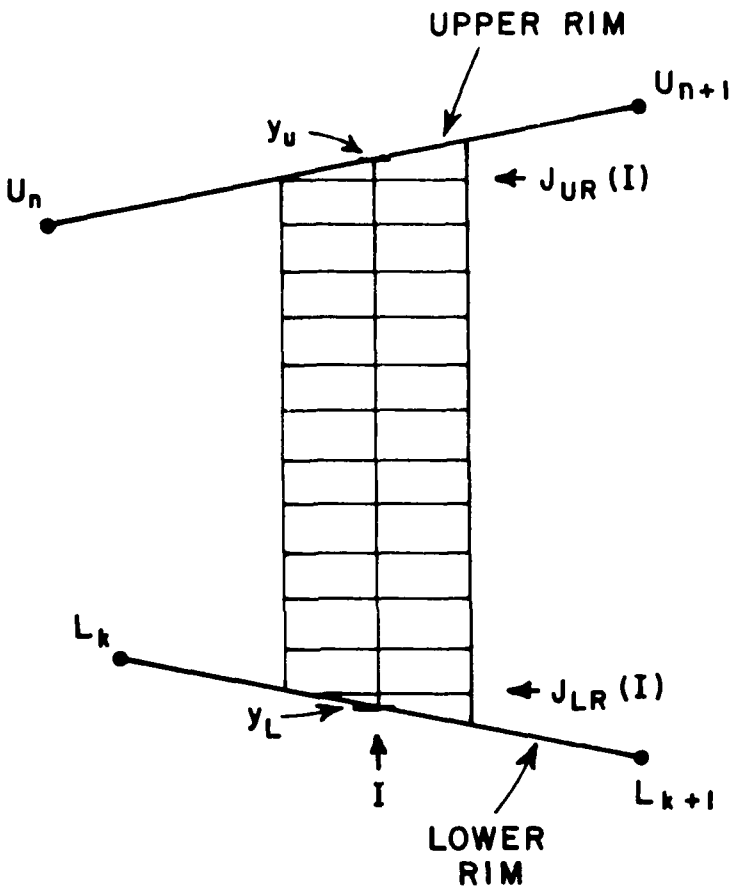

Figure 8. Lower and upper horizontal grid lines for y-integration.

TABLE III

Subaperture Type N	Interval for $x-x_o$	Interval for $y-y_o$	Element Pattern $F_{SN}(\theta,\phi)$
0	(-dx,+dx)	(-dy,+dy)	dx dy $F_F(\phi x)\ F_F(\phi y)$
1	(-dx,+dx)	(0.+dy)	dx dy $F_F(\phi x)\ F_H(\phi y)$
2	(-dx,+dx)	(-dy,0)	dx dy $F_F(\phi x)\ F_H(-\phi y)$
3	(0.+dx)	(-dy,+dy)	dx dy $F_H(+\phi x)\ F_F(\phi y)$
4	(-dx,0)	(-dy,+dy)	dx dy $F_H(-\phi x)\ F_F(\phi y)$

In order to treat the subapertures along the reflector rim, four other types of subapertures are introduced as shown in Figure 7b. The area of each additional type is one-half of that for the basic subaperture (type 0). The field distribution for each type is the same as that given by Equation (1) except for different x and y intervals as given in Table III. The corresponding element patterns can be expressed in terms of the one-dimensional pattern functions: $F_F(\phi s)$ for a full triangular distribution, $f_F(s)$, and $F_H(\phi s)$ for a half triangular distribution, $f_H(s)$, as shown in Figure 9. Thus

Figure 9. Triangular subaperture distributions (full and half).

$$F_F(\phi s) = \left[\frac{\sin(\frac{\phi s}{2})}{(\frac{\phi s}{2})}\right]^2 \qquad (3)$$

and

$$F_H(\phi s) = \frac{1 - e^{j\phi s}}{(\phi s)^2} + \frac{j}{\phi s} \qquad (4)$$

The resulting element patterns $F_{SN}(\theta,\phi)$ for each type are also given in Table III.

The y integration is divided into 3 parts: the lower part usually consists of the contribution of the Type 1 subaperture at the lower rim and the upper part is usually one subaperture of Type 2 at the upper rim. Types 3 and 4 are used for the lower and upper parts when the reflector rim has a steep slope. The subapertures in the middle part are the basic Type 0. The Type 3 subaperture is used exclusively along the left side of the rim ($I = 1$); and the Type 4 is used on the right side ($I = I_{max}$), as shown in Figure 7b.

Dividing the y integration into 3 parts has the significant advantage that the product of the aperture field and phase exponential for each subaperture can be simply summed for each integation part. The result for each part of the y-integration is then multiplied by the element pattern $F_{SN}(\theta,\phi)$ of the appropriate Type N. Thus the contribution from each part can be expressed as

$$Ys = F_{SN}(\theta,\phi) \sum_{J=J_I}^{J_F} Ea\,(Ix\,dx, Jy\,dy)\, e^{j\,Jy\,\phi y} \qquad (5)$$

where $Ix = I - Ic$ and $Jy = J - Jc$.

The exponential in Equation (5) provides the y component of the phase reference for each subaperture. The lower limit J_I and the upper limit J_F are given in Table IV for each integration part, where N_{LG} and N_{UG}

TABLE IV

y-Integration Part	Subaperture Type	Subaperture Number	Limit Lower (J_I)	Limit Upper (J_F)
lower (Y_{SL})	$N = N_{LW}$ (usually 1)	N_{LG} (usually 1)	$J_{LR}(I)$	$J_{LR}(I)+N_{LG}-1$
Middle (Y_{SM})	$N = 0$	(Remaining)	$J_{LR}(I)+N_{LG}$	$J_{UR}(I)-N_{UG}$
Upper (Y_{SU})	$N = N_{UP}$ (usually 2)	N_{UG} (usually 1)	$J_{UR}(I)-N_{UG}+1$	$J_{UR}(I)$

are the number of subapertures in the lower and upper parts, respectively. The values of N_{LG} and N_{UG} are usually unity except for very steep slopes of the reflector rim, where the subaperture Types N_{LW} and N_{UP} may be chosen as 3 or 4 to better fit the aperture rim shape. As previously mentioned, Type 3 is used exclusively for the first vertical grid line ($I = 1$); and Type 4 is used for the final grid line ($I = I_{max}$). The y-integration sum is thus given by

$$Y_{SUM}(I) = Y_{SL} + Y_{SM} + Y_{SU} \cdot \tag{6}$$

The 2-D aperture integration is completed by summing on I; thus the rectangular subaperture method gives the far field pattern as

$$F(\theta,\phi) = \sum_{I=1}^{Imax} Y_{SUM}(I)\, e^{j(Ix)\phi x} \tag{7}$$

where the exponential in Equation (7) provides the x component of the phase reference. Equation (7) represents the principally-polarized component which is dominant in the main beam region. When the present far field code is delivered to NOSC early in the second year's program, it will include the cross-polarized component and hence the total field.

B. Program Performance Specification (PPS) for Reflector Antenna Code/Far Field w/o Blockage

The objective of the computer code is to provide the capability for calculating the far field (FF) patterns for typical Navy reflector antennas. The theoretical approach for computing the far field pattern of the general reflector is based on a combination of the Geometrical Theory of Diffraction (GTD) and Aperture Integration (AI) techniques. AI is used to compute the main beam and near sidelobes; GTD is used to compute the wide-angle sidelobes and the backlobes.

The code provides the following capabilities:

1. Reflector surfaces may be either paraboloidal or cylindrical-parabolic.

2. A general reflector rim shape may be used (piece-wise linear up to 100 segments).

3. The required input data for the feed pattern is minimized by polynomial and piece-wise linear pattern fitting.

4. Storage and computation time of aperture data for AI is minimized by a rectangular subaperture method.

5. The efficiency of the far field pattern computation is maximized by the use of GTD for wide pattern angles and the use of the rectangular subaperture method for near-axis angles (main beam region).

An outline of the code is given in Table V. Formats for input and output data are given in Tables VI and VII, respectively.

TABLE V
OUTLINE OF COMPUTER CODE

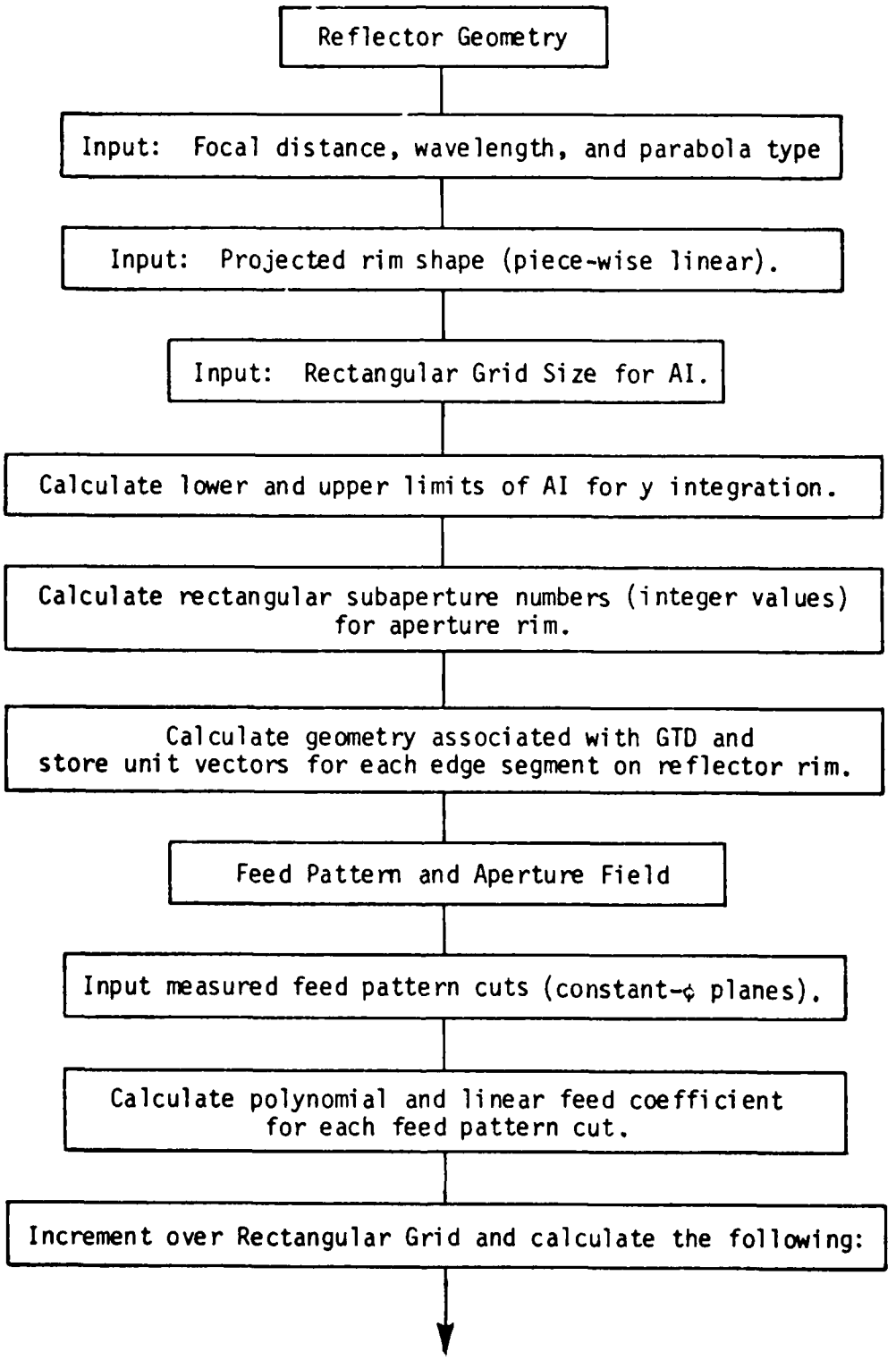

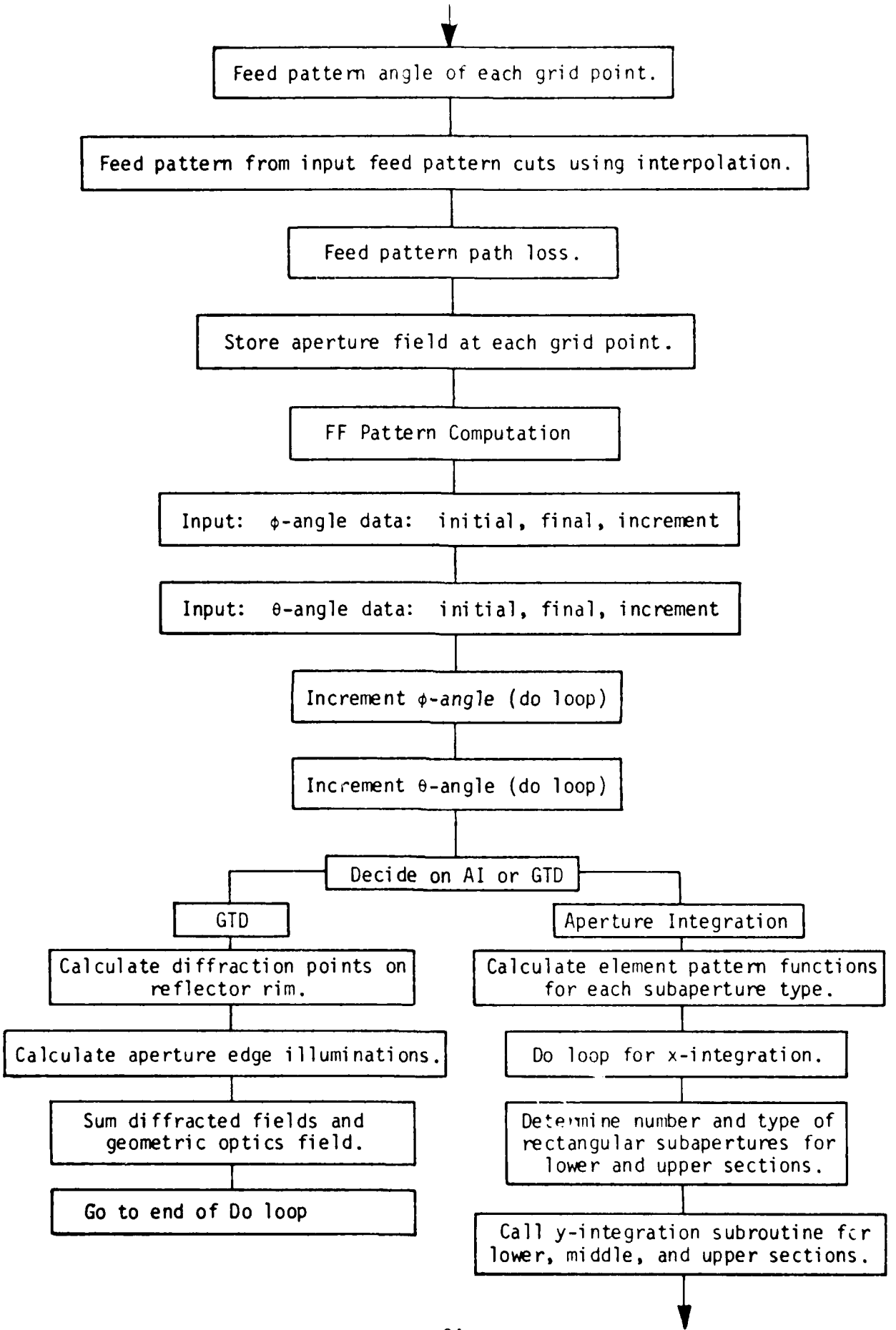
Feed pattern angle of each grid point.
Feed pattern from input feed pattern cuts using interpolation.
Feed pattern path loss.
Store aperture field at each grid point.
FF Pattern Computation
Input: φ-angle data: initial, final, increment
Input: θ-angle data: initial, final, increment
Increment φ-angle (do loop)
Increment θ-angle (do loop)
Decide on AI or GTD
GTD
Calculate diffraction points on reflector rim.
Calculate aperture edge illuminations.
Sum diffracted fields and geometric optics field.
Go to end of Do loop
Aperture Integration
Calculate element pattern functions for each subaperture type.
Do loop for x-integration.
Determine number and type of rectangular subapertures for lower and upper sections.
Call y-integration subroutine for lower, middle, and upper sections.

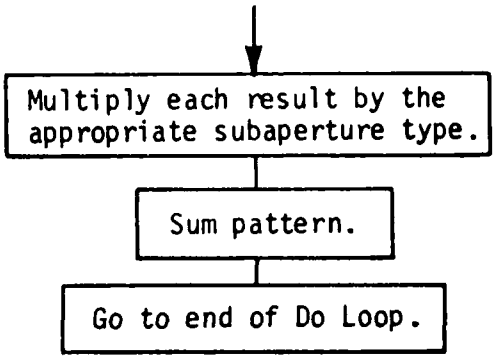

Y-integration Subroutine

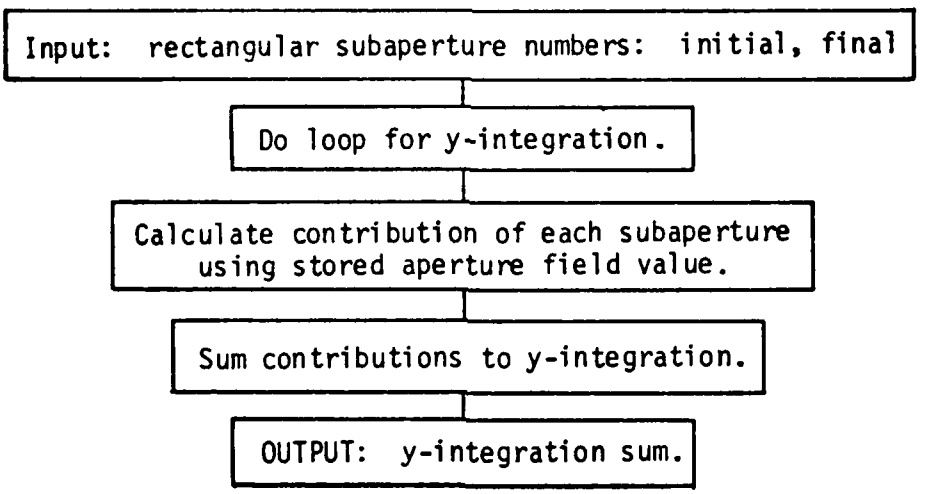

TABLE VI

FORMAT OF INPUT

INPUT	Dimension	Wavelength
Choose dimension units and input all linear dimensions in same units i.e. Focal distance Rectangular grid size	inches meters or wavelengths	λ inches λ meters $\lambda = 1$

Projected rim shape: Coordinates (X_n, Y_n) of junction between each piecewise linear segment

Parabola Type: Paraboloidal: Type 1 (NREFL = 1)

Cylindrical: Type 2 (NREFL = 2)

Input all angles in degrees:

FF Pattern angle data: θ, ϕ

Feed Pattern: Pattern level in dB: $f(\psi, \phi)$
Angles in degrees: ψ, ϕ

TABLE VII
FORMAT OF OUTPUT

All input data for information and checking.

Complete feed pattern as calculated from input feed data.
ϕ,ψ in degrees; $f(\psi,\phi)$ in dB
Calculated aperture field data

Output FF Pattern

ϕ-angle = degrees

Pattern Angle	FF Pattern			
	θ Component		ϕ Component	
θ degrees	dB	Phase	dB	Phase
-	-	-	-	-
-	-	-	-	-
-	-	-	-	-

Estimated Machine Storage Required: 200 K bytes

V. THEORETICAL STUDIES

In the present period work on the derivation of diffraction coefficients for a perfectly-conducting circular cylinder of radius a was completed. This diffraction coefficient is particularly useful and numerically efficient as $ka \to 0$; furthermore, it may be used when the axis of the cylinder is curved as in the case of a bent wire. The dyadic (or matrix) form of the diffraction coefficient is the same as that of a curved wedge, which is not surprising since both structures involve lines of scattering (the axis of the cylinder and the edge of the wedge). Although diffraction coefficients were obtained only for cylinders of circular cross section, the method of solution can be readily extended to perfectly-conducting cylinders of arbitrary cross section and to penetrable cylinders, provided that the maximum extent of the cylinder cross section is not large in terms of a wavelength.

The diffraction coefficient for the circular cylinder was employed to calculate the radiation pattern of a LAMPS antenna with a cylindrical mast in front of it. A separate report has been written describing this work [1].

Work on the GTD analysis of the scattering by two staggered, parallel half-planes (plates) referred to in the March monthly report has been extended to the case where the interacting edges form a thick edge, a geometry more likely to be encountered in practice. As in the case of the staggered half planes, the second edge is positioned on the shadow boundary of the first. Some difficulties have been encountered when the second edge is in the transition region of the first edge (but not on its shadow boundary), and the field point lies in the transition region of the second edge. It is a matter of reducing a double integral to a form suitable for numerical results. Also in the present period we were concerned about the complex angles of incidence which occur in our integral representations of the diffracted field. In particular, could we justify the use of diffraction coefficients with complex angles of incidence? We have examined this point carefully, and modified our approach so that this difficulty appears to be overcome.

In the period ahead we plan to return to the task of completing the report on slope diffraction.

REFERENCE

[1] R. G. Kouyoumjian, R. G. Luebbers, and R.C. Rudduck, "A GTD Analysis of the LAMPS Antenna Blocked by a Mast," Report 4508-3, (in preparation), The Ohio State University ElectroScience Laboratory, Department of Electrical Engineering; prepared under Contract N00123-76-C-1371 for Naval Regional Procurement Office, Long Beach, California 90822.

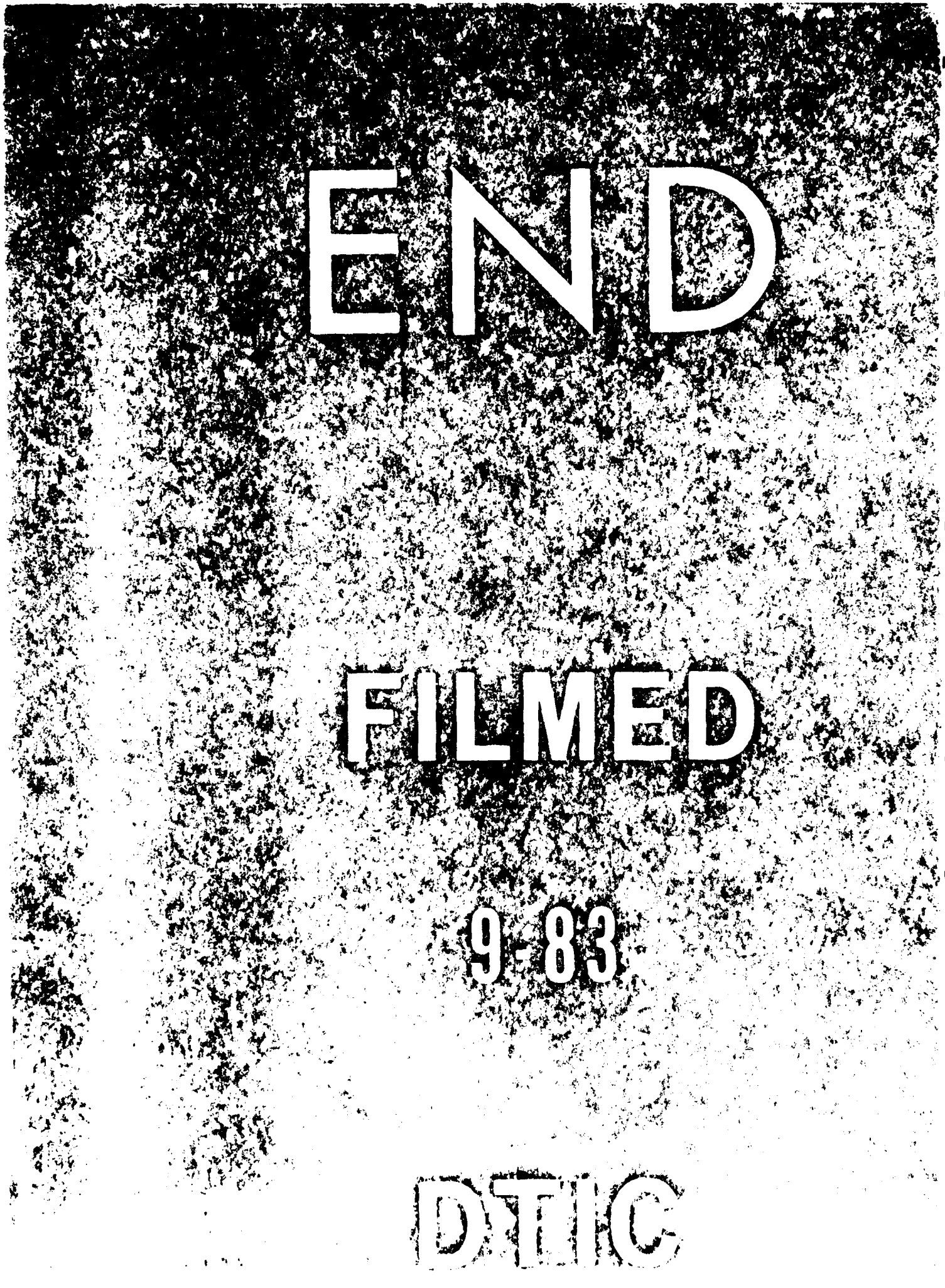
END
FILMED
9-83
DTIC